Control of a mechatronics-assisted system for surgeries using flexible tools*

Lingbo Cheng, *student Member, IEEE,* Mahdi Tavakoli, *Member, IEEE*

***Abstract*—Flexible and lightweight surgical tools have the potential to significantly increase the dexterity of mechatronics-assisted surgical systems for minimally invasive surgeries. However, the control of a mechatronics-assisted system with the link and joint flexibility is quite challenging and needs to be studied. In this paper, a bilateral impedance-controlled master-slave teleoperation system is considered, where the slave (surgical) robot is flexible. Two reference impedance models are designed for the master and slave robots to control the mechatronics-assisted system. Also, depending on different feedback and feedforward signals, four cases are distinguished. To obtain better transparency of the system, the tuning rules for the impedance parameters for each case are presented and the corresponding transparency measures are analyzed and compared. As a result, by appropriately adjusting the impedance model parameters, ideal position and force tracking can be attained for a teleoperation system with a flexible surgical robot. The theoretical findings are validated in simulations.**

I. Introduction

Mechatronic-assisted robotic systems have been employed for surgery to assist the surgeon in performing a surgical procedure which may require the robotic system to have a large variety of extent of automation. Robotic systems for surgery can be classified into three main categories depending on the degree of autonomy granted to it: fully autonomous robotic system, high-level, semi-autonomous robotic system, and low-level, semi-autonomous robotic system.

A typical fully autonomous surgical robot is surgical computer aided design or computer aided manufacturing [1] which is using a computer to realize the process of building the patient model, planning, registration, execution, and follow-up. The preprogrammed robotic systems provide advantages and convenience to surgical procedures. However, not all surgical robotics are designed to replace the surgeon. In fact, most of them are designed to assist the surgeon by providing with versatile tools to extend the surgeon's operation ability. This kind of surgical robotics are semi-autonomous and can be classified by level of autonomy. The high-level semi-autonomous surgical systems generally work side-by-side with the surgeon and provide a joystick or foot pedal to permit the surgeon to control the motion of the surgical systems [2]. The low-level, semi-autonomous surgical systems are operated directly by the surgeon to extend his/her ability such as the elimination of hand tremor [3] and can be used for remote surgery. A typical example is the teleoperation surgical system [4] (e.g. the da Vinci system from Intuitive Surgical Inc., Sunnyvale, CA) where a surgeon interacts with a master robot to perform a desired task on the target tissue by a slave robot (surgical robot). This system can be used to perform minimally invasive surgeries (MIS) [5] with advantages such as small incisions reduce pain and short rehabilitation time.

The dexterity of mechatronic-assisted surgical robots for MIS can be enhanced by using flexible and lightweight tools such as needles, endoscopes, and catheters, while also reducing trauma, which is a benefit for post-operative recovery [6]. Nevertheless, the requirements of such flexible tools make traditional teleoperation control methods [7]–[9], which are for rigid robots, no longer sufficient as flexibility caused by the limited stiffness of transmission mechanisms at the robot joints and the deflection of links may lead to problems such as transient errors, vibrations, and instability [10]. Moreover, for a master-slave teleoperation system, the introduction of slave robot flexibility will inevitably affect the transparency of the system, which consequently reduces the accuracy of position and force tracking performance.

To this end, various control strategies have been proposed for teleoperation system with a flexible slave. In [11], a position-exchange controller for the bilateral teleoperation of flexible surgical robots was proposed. By assuming the master manipulator as a one-degree-of-freedom (1-DOF) rigid link and the slave manipulator as a 1-DOF elastic link and using the position of the master robot and the deformed shape of the flexible slave robot, the controller enabled the master robot to follow the position of the slave robot. In [12], the authors developed a more realistic model for slave link deflections and used the Extended Lawrence Four-Channel control architecture for the teleoperation system. In our previous work [13], to study the effect of a flexible robot on the conventional position error based (PEB) teleoperation and direct force reflection (DFR) teleoperation, the flexible slave manipulator with a flexible link was modeled as a linear joint stiffness. In [13], we analyzed the transparency measures for the two systems and concluded that perfect position and force tracking might be possible assuming the control gains were infinity.

This paper builds on previous work of the authors [7][13] and developed a impedance-controlled mechatronic-assisted system for surgeries with flexible tools, which includes two impedance models for the master and slave robots, respectively. In the context of teleoperated bilateral impedance control, depending on different feedback and feedforward signals between the master and slave robots, the effect of slave flexibility and the impedance model parameters on the transparency of the system is studied.

*The authors are with the Department of Electrical and Computer Engineering, University of Alberta, Edmonton, AB T6G 1H9, Canada. (e-mails: lingbo1@ualberta.ca, mahdi.tavakoli@ualberta.ca).

978-1-7281-0355-6/19/$31.00 ©2019 IEEE

II. System Control Method

For a teleoperation system in Fig. 1, bilateral impedance control can be applied by designing two reference impedance models for the master and slave robots, respectively.

By adjusting the parameters of the reference impedance models appropriately, desired dynamical relations between the external forces and the robot positions can be attained. In Fig. 1, f_h is the human-master contact force, and f_e is the slave-environment contact force. Also, x_m and x_s are the positions of the master and slave robots, respectively. The reference impedance models for the master and slave robots provide desired response positions x_{ref_m} and x_{ref_s} to the master and slave position controllers, respectively, so that the robots' trajectories will follow the desired positions (ideally, $x_m = x_{ref_m}$, $x_s = x_{ref_s}$). Note that u_m and u_s are the control signals for the master and slave robots. The position controllers for the two robots are designed as proportional-derivative (PD) controllers. As the stiffness and damping terms in the dynamics of the robots would contribute to the closed-loop equations in the same way as the proportional and derivative terms of the PD position controllers, the dynamics of the robots in the following only involve the inertia terms.

A. Criteria for Analysis of Teleoperation Performance

For a transparent teleoperation system, the ideal goals are

$$x_m = x_s, \quad f_h = f_e \tag{1}$$

The relationship between the master the and slave quantities in (1) can be expressed in the s-domain as

$$\begin{bmatrix} F_h(s) \\ -X_s(s) \end{bmatrix} = \underbrace{\begin{bmatrix} 0 & 1 \\ -1 & 0 \end{bmatrix}}_{H} \begin{bmatrix} X_m(s) \\ F_e(s) \end{bmatrix} \tag{2}$$

where the matrix H includes the ideal hybrid parameters. We mainly consider two elements in the matrix H to analyze the teleoperation transparency:

$$h_{11} = \frac{F_h}{X_m}\Big|_{F_e=0}, \qquad h_{21} = -\frac{X_s}{X_m}\Big|_{F_e=0} \tag{3}$$

Here, h_{11} is the human operator perceived impedance when the slave is moving freely, and h_{21} is the position tracking fidelity when the slave is moving freely. The ideal values for these two measures are 0 and -1, respectively. Also, we consider two more measures:

$$f_{12} = \frac{F_h}{F_e}\Big|_{X_s=0}, \qquad z_{11} = \frac{F_h}{X_m}\Big|_{X_s=\text{const}} \tag{4}$$

In the above, f_{12} is the force tracking fidelity when the slave contacts a hard environment, and z_{11} is the human operator's perceived maximum impedance. The ideal values for these two measures are 1 and ∞, respectively.

B. Flexible Slave Model

In Fig. 1, the flexible slave robot can be considered as having a flexible coupling between its motor (actuator) and end-effector (surgical tool). For a 1-DOF system, it has been proved that a flexible link and a flexible joint have similar effects on teleoperation performance [14]. The dynamics of the flexible link are identical to the dynamics of the flexible joint shown in Fig. 2 consisting of a motor and an end-effector

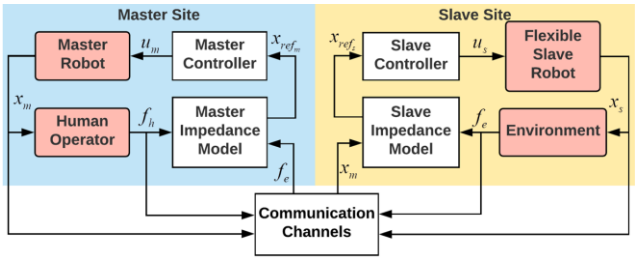

Figure 1. The bilateral impedance-controlled teleoperation system.

that are coupled via a shaft with a finite stiffness. Specifically, two masses connected by a spring are used to model a rotational elastic joint (Fig. 2(a)). By using the equivalent translational model of the flexible joint, the model shown in Fig. 2(a) can be represented by the model shown in Fig. 2(b).

In Fig. 2(b), the motion equations of the flexible joint are

$$M_{sm}\ddot{x}_{sm} + k_{fs}\Delta x_s = f_s \tag{5}$$

$$M_{se}\ddot{x}_{se} - k_{fs}\Delta x_s = -f_e \tag{6}$$

$$\Delta x_s = x_{sm} - x_{se} \tag{7}$$

C. Models of the System with Flexible-Joint Slave Robot

The models of the bilateral impedance-controlled teleoperation system with a flexible-joint slave are presented in Fig. 3. The reference impedance models for the master and slave robots are denoted by Z_m and Z_s, respectively. The parameters m_i, c_i, and k_i are the inertia, damping, and stiffness of the reference impedance model. The subscript $i = m$ is for the master, and $i = s$ is for the slave. Also, C_m and C_s are PD position controllers for the master and slave robots,

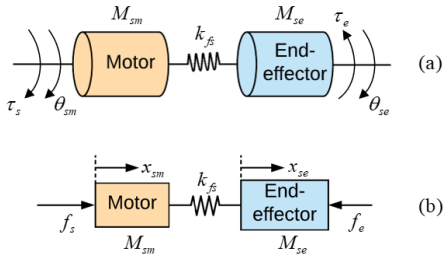

Figure 2. (a) Model of a flexible joint. (b) An equivalent representation of the flexible joint model. Here, M_i, θ_i, and x_i are the inertia, angle, and position. The subscript $i = sm$ is for the motor and $i = se$ is for the end-effector. Also, k_{fs} is the flexible joint's stiffness, τ_s and τ_e are the motor torque (control signal) and the torque applied by the environment, and f_s and f_e are the motor force and the force applied by the environment.

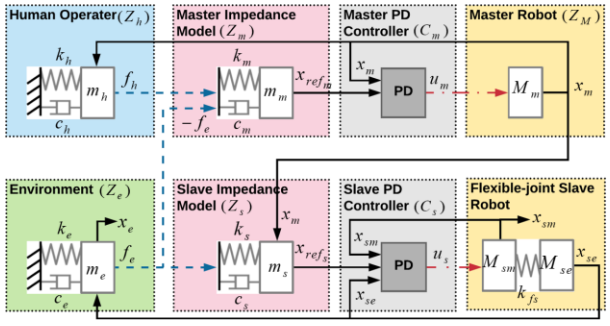

Figure 3. The models of the bilateral impedance-controlled teleoperation system with flexible-joint slave robot. The solid and dashed lines indicate the position and force transfer paths, respectively.

respectively. The control signals u_m and u_s are applied to the robots and result in the movements of the robots. The inertia of the master robot is denoted by M_m.

In Fig. 3, the human operator applies forces, f_h, on the master robot, which is an input to the reference impedance model for the master robot. This reference model also receives the slave-environment contact forces, f_e, and generates the desired position for the master robot controller which controls the master robot to track the desired position, x_{ref_m}. On the slave site, the reference impedance model for the slave robot receives the inputs of slave-environment contact forces, f_e, and the master robot position, x_m, and generates the desired position for the slave robot controller, x_{ref_s}. The desired impedance models for the master and slave robots are

$$m_m\ddot{x}_{ref_m} + c_m\dot{x}_{ref_m} + k_m x_{ref_m} = f_h - f_e \tag{8}$$

$$m_s\ddot{\tilde{x}}_{ref_s} + c_s\dot{\tilde{x}}_{ref_s} + k_s\tilde{x}_{ref_s} = -f_e \tag{9}$$

where $\tilde{x}_{ref_s} = x_{ref_s} - x_m$ is the error of the slave impedance model's response with respect to the master robot position. The objective of model (9) is decreasing the error $\tilde{x}_{ref_s}$ so that x_{ref_s} follows x_m. Here, x_{ref_s} is the reference position for the flexible slave. When x_{ref_s} is the reference position for the slave motor x_{sm}, the position of the slave end-effector x_{se} may not accurately follow the master robot position x_m. To achieve perfect position tracking between the slave end-effector x_{se} and the master robot x_m, $\tilde{x}_{ref_s}$ should be adjusted. By combining (6) and (7), x_{sm} is given by

$$x_{sm} = x_{se} + \frac{f_e}{k_{fs}} + \frac{m_{se}}{k_{fs}}\ddot{x}_{se} \tag{10}$$

Since the desired position of the slave end-effector x_{se} is x_m, the reference trajectory for x_{sm} becomes

$$x_m^* = x_m + \frac{f_e}{k_{fs}} + \frac{m_{se}}{k_{fs}}\ddot{x}_m \tag{11}$$

Therefore, the adjusted position error in (9) is

$$\tilde{x}_{ref_s} = x_{ref_s} - x_m^* \tag{12}$$

D. Framework Overview

The *s*-domain representation of the impedance- controlled teleoperation system is presented in Fig. 4. With the designed impedance models for the master and slave robots, we have $C_1 = Z_s$, $C_2 = 1$, $Z_m^{-1} = \frac{1}{m_m s^2 + c_m s + k_m}$, and $Z_s^{-1} = \frac{1}{m_s s^2 + c_s s + k_s}$. Also, the master robot, the slave motor, and the slave end-effector are represented as the impedance $Z_M^{-1} = \frac{1}{M_m s^2}$, $Z_{sm}^{-1} = \frac{1}{M_{sm} s^2}$, and $Z_{se}^{-1} = \frac{1}{M_{se} s^2}$, respectively. The PD position controllers C_m and C_s (corresponding to the rigid slave) are expressed as

$$C_m = k_{d_m} s + k_{p_m}, \quad C_s = k_{d_s} s + k_{p_s} \tag{13}$$

In the present of flexible-joint slave, C_s is broke into two separate controllers C_{sm} and C_{se}. In addition, C_3 and C_4 are two position gains. The control laws for the master and slave robots are given by

$$U_m = C_3 X_{ref_m} - C_m X_m \tag{14}$$

$$U_s = C_4 X_{ref_s} - C_{sm} X_{sm} - C_{se} X_{se} \tag{15}$$

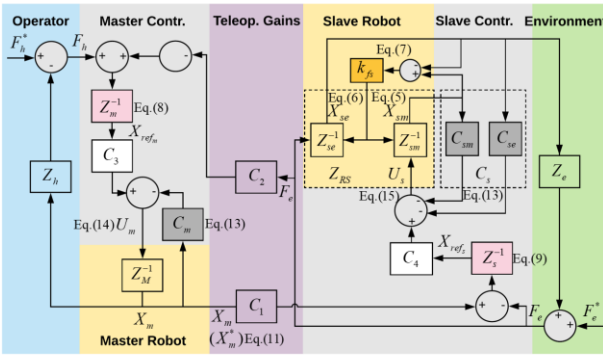

Figure 4. The bilateral impedance-controlled teleoperation architecture.

where C_{sm} and C_{se} are PD position controllers for the slave motor and the slave end-effector. Generally, $C_3 = C_m$ and $C_4 = C_s$ are designed to achieve position tracking. For simplicity, in this paper $C_m = C_s = C_{sm} = C_{se} = k_d s + k_p$ is chosen, where $k_d = 2\alpha M_{sm}$ and $k_p = \alpha^2 M_{sm}$ ($\alpha > 0$) are designed to guarantee critical damping.

Based on the possible communication signals for both feedback and feedforward, four cases are distinguished and listed in Table I. The position and the external force of the slave end-effector x_{se} and f_e may be difficult to be measured directly by sensors. Therefore, an extended state observer may be used to estimate these quantities [15][16] so that all variables are available in each case.

III. Transparency Measures

To simplify the expressions of the results, some substitutions are introduced $\omega_0 = \sqrt{\frac{k_{fs}}{M_{se}}}$, $R_s = \frac{M_{se}}{M_{sm}}$, $r_s = \frac{m_s}{M_{sm}}$, $r_m = \frac{m_m}{M_{sm}}$. For the reference impedance models Z_m and Z_s, the natural frequencies and the damping ratios are given by $\omega_m = \sqrt{k_m/m_m}$, $\omega_s = \sqrt{k_s/m_s}$, and $\zeta_m = c_m/2\sqrt{m_m k_m}$, $\zeta_s = c_s/2\sqrt{m_s k_s}$, respectively. Assuming $\zeta_m = \zeta_{sm} = 1$, we have $Z_m = m_m(s+\omega_m)^2$ and $Z_s = m_s(s+\omega_s)^2$. Therefore, the adjustable parameters are r_m, r_s, ω_m, and ω_s.

A. Rigid Case

When the slave is rigid, to achieve better performance, $C_3 = Z_M + C_m$ and $C_4 = Z_{RS} + C_s$ are chosen, where Z_{RS} ($= \frac{1}{M_s s^2}$, where M_s is the inertia of the rigid slave robot) denotes the impedance of the rigid slave robot. As a result, the performance measures are $h_{11} = Z_m$, $h_{21} = -1$, $\frac{1}{f_{12}} = \frac{Z_s}{Z_m + Z_s}$, $z_{11} = Z_m + Z_s$. To ensure the transfer function is proper, $1/f_{12}$ is used. If the impedance models for the master and slave robots are chosen to be $Z_m = 0$ and $Z_s = \infty$, the above performance measures will equal the ideal values.

TABLE I. Possible Communication Signals

Communication Signals	Case 1	Case 2	Case 3	Case 4
Feedback	x_{sm}, f_e	x_{sm}, f_e	x_{se}, f_e	x_{sm}, x_{se}, f_e
Feedforward	x_m	x_m^*	x_m	x_m^*, x_m

B. Flexible Case 1

For flexible case, as the slave robot includes two parts, $C_4 = \lambda_1 Z_{sm} + \lambda_2 Z_{se} + C_{sm} + C_{se}$ is chosen, where λ_1 and λ_2 are two coefficients, which can be selected as $\lambda_1 = 1$ and $\lambda_2 = 0$, for simplicity. In case 1, with feedback of x_{sm}, C_{se} is zero and $C_4 = Z_{sm} + C_{sm}$. Also, $C_3 = Z_M + C_m$ is chosen. Note that given the flexible salve model (5)-(7), the slave position X_s defined in (3) and (4) should be changed as the position of the slave end-effector x_{se}. The transparency measures are $h_{11} = Z_m$, $h_{21} = \frac{-1}{1+\left(\frac{s}{\omega_0}\right)^2+R_s\left(\frac{s}{s+\alpha}\right)^2}$, $\frac{1}{f_{12}} = \frac{1}{1+\frac{r_m}{r_s}\left(\frac{s+\omega_m}{s+\omega_s}\right)^2+\frac{r_m}{R_s}\left(\frac{s+\omega_m}{\omega_0}\right)^2+r_m\left(\frac{s+\omega_m}{s+\alpha}\right)^2}$, $z_{11} = Z_m + m_s \frac{(s+\omega_s)^2}{1+\frac{r_s}{R_s}\left(\frac{s+\omega_s}{\omega_0}\right)^2+r_s\left(\frac{s+\omega_s}{s+\alpha}\right)^2}$. If the stiffness of the flexible spring k_{fs} is sufficiently large and the inertia rate R_s is sufficiently small, h_{21} will equal -1, which matches the measure in the rigid case.

C. Flexible Case 2

With feedback of x_{sm} and feedforward of x_m^*, the controllers remain the same as those in Case 1. The four transparency measures are $h_{11} = Z_m$, $h_{21} = -\frac{1+\left(\frac{s}{\omega_0}\right)^2}{1+\left(\frac{s}{\omega_0}\right)^2+R_s\left(\frac{s}{s+\alpha}\right)^2}$, $\frac{1}{f_{12}} = \frac{1+\left(\frac{s}{\omega_0}\right)^2}{1+\left(\frac{s}{\omega_0}\right)^2+\frac{r_m}{r_s}\left(\frac{s+\omega_m}{s+\omega_s}\right)^2+r_m\left(\frac{s+\omega_m}{s+\alpha}\right)^2}$, $z_{11} = Z_m + m_s \frac{(s+\omega_s)^2\left(1+\left(\frac{s}{\omega_0}\right)^2\right)}{1+r_s\left(\frac{s+\omega_s}{s+\alpha}\right)^2}$.

D. Flexible Case 3

With feedback of x_{se}, it can be noted that C_{sm} is zero. Hence, $C_4 = Z_{sm} + C_{se}$. Also, $C_3 = Z_M + C_m$ is chosen. The four transparency measures in this case are $h_{11} = Z_m$, $h_{21} = \frac{-1}{1+\left(R_s+\left(\frac{s}{\omega_0}\right)^2\right)\left(\frac{s}{s+\alpha}\right)^2}$, $\frac{1}{f_{12}} = \frac{1}{1+\frac{r_m}{r_s}\left(\frac{s+\omega_m}{s+\omega_s}\right)^2+r_m\left(\frac{s+\omega_m}{s+\alpha}\right)^2\left(1+\frac{1}{R_s}\left(\frac{s}{\omega_0}\right)^2\right)}$, $z_{11} = Z_m + m_s \frac{(s+\omega_s)^2}{1+r_s\left(\frac{s+\omega_s}{s+\alpha}\right)^2\left(1+\frac{1}{R_s}\left(\frac{s}{\omega_0}\right)^2\right)}$.

E. Flexible Case 4

With feedback of x_{sm}, x_{se} and feedforward of x_m^*, x_m, the reference impedance models for the slave motor and the slave end-effector are given by

$$m_s\ddot{\tilde{x}}_{ref_{sm}} + c_s\dot{\tilde{x}}_{ref_{sm}} + k_s\tilde{x}_{ref_{sm}} = -f_e \quad (13)$$

$$m_s\ddot{\tilde{x}}_{ref_{se}} + c_s\dot{\tilde{x}}_{ref_{se}} + k_s\tilde{x}_{ref_{se}} = -f_e \quad (14)$$

where $\tilde{x}_{ref_{sm}} = x_{ref_{sm}} - x_m^*$ and $\tilde{x}_{ref_{se}} = x_{ref_{se}} - x_m$. Note that $x_{ref_{sm}}$ is the reference trajectory for the slave motor x_{sm}, and $x_{ref_{se}}$ is the reference trajectory for the slave end-effector x_{se}. In addition, C_4 is replaced by C_{4sm} and C_{4se}. The control law for the flexible slave robot is defined as $U_s = C_{4sm}X_{ref_{sm}} + C_{4se}X_{ref_{se}} - C_{sm}X_{sm} - C_{se}X_{se}$, where $C_{4sm} = Z_{sm} + C_{sm}$, and $C_{4se} = Z_{se} + C_{se}$. The resulting four measures of transparency are $h_{11} = Z_m$, $h_{21} = -1$, $\frac{1}{f_{12}} = \frac{2+(R_s-1)\left(\frac{s}{s+\alpha}\right)^2+\left(\frac{s}{\omega_0}\right)^2}{\left(1+\frac{r_m}{r_s}\left(\frac{s+\omega_m}{s+\omega_s}\right)^2\right)\left(2+(R_s-1)\left(\frac{s}{s+\alpha}\right)^2\right)+\left(\frac{s}{\omega_0}\right)^2+r_m\left(\frac{s+\omega_m}{s+\alpha}\right)^2}$, $z_{11} = Z_m + m_s \frac{(s+\omega_s)^2\left(2+\left(\frac{s}{\omega_0}\right)^2+(R_s-1)\left(\frac{s}{s+\alpha}\right)^2\right)}{2+r_s\left(\frac{s+\omega_s}{s+\alpha}\right)^2+(R_s-1)\left(\frac{s}{s+\alpha}\right)^2}$.

IV. Transparency Analysis

A. Transparency with no Actuator Saturation

By assuming the control gain α is infinitely large, the idealized transparency measures for the four flexible cases are listed in Table II, which present that perfect free-motion position tracking can be attained. For Case 1, position tracking is satisfactory only at low frequencies ($\omega < \omega_0$), while for the other cases, position tracking is satisfactory without frequency limitations. For hard-contact force tracking ($1/f_{12}$), it can be noted that the term of $P = \frac{r_m}{r_s}\left(\frac{s+\omega_m}{s+\omega_s}\right)^2$ is involved in every denominator of the four cases. If P can be adjusted to be zero, perfect hard-contact force tracking can be achieved (For Case 1, force tracking is satisfactory at low frequencies; for other cases, force tracking is satisfactory at any frequencies).

B. Parameter Adjustment for Robot Impedance Models

To find the effect of r_m, r_s, ω_m, and ω_s on the shape of $1/f_{12}$, as an example, the magnitudes of $1/f_{12}$ for case 3 are plotted in Fig. 5(a) when r_m/r_s = 1, 0.5, 0.1, ω_s = 100 rad/s, ω_m = 1, 50, 100 rad/s. Furthermore, when r_m/r_s is constant, small ω_m brings $1/f_{12}$ closer to the ideal value 1 (Fig. 5(b)).

When ω_m is constant, small r_m/r_s not only brings $1/f_{12}$ closer to the ideal value 1, but also provides a wider frequency range of force tracking (Fig. 5(c)). Therefore, the frequency range of ω_m can be improved by decreasing r_m/r_s. In other words, if $\omega_m = \omega_s$ is desired, r_m/r_s has to be very small.

C. Position Tracking Considering Actuator Saturation

In practice, however, the control gain α cannot be infinitely large, which will inevitably influence the system's transparency measures. To investigate the effect of α on the shape of position tracking, the magnitudes of h_{21} are plotted in Fig. 6 when ω_0 = 100 rad/s, R_s = 0.1 (lightweight slave end-effector), and α = 1, 100, 10000. For Case 1 and 2, regardless of the control gain α, position tracking is attained only at low frequencies ($\omega < \omega_0$). Also, the frequency range of position tracking for Case 2 is a bit wider than that for Case 1. In Case 3 the position tracking performance is better than the first two

TABLE II. Idealized Transparency Measures

Item	h_{11}	h_{21}	$1/f_{12}$	z_{11}
Case 1	Z_m	$\frac{-1}{1+\left(\frac{s}{\omega_0}\right)^2}$	$\frac{1}{1+P+\frac{r_m}{R_s}\left(\frac{s+\omega_m}{\omega_0}\right)^2}$	$Z_m+\frac{Z_s k_s}{Z_s+k_s}$
Case 2	Z_m	-1	$\frac{1+\left(\frac{s}{\omega_0}\right)^2}{1+\left(\frac{s}{\omega_0}\right)^2+P}$	$Z_m+Z_s\left(1+\left(\frac{s}{\omega_0}\right)^2\right)$
Case 3	Z_m	-1	$\frac{1}{1+P}$	Z_m+Z_s
Case 4	Z_m	-1	$\frac{2+\left(\frac{s}{\omega_0}\right)^2}{2(1+P)+\left(\frac{s}{\omega_0}\right)^2}$	$Z_m+Z_s\left(1+\frac{1}{2}\left(\frac{s}{\omega_0}\right)^2\right)$
Ideal Value	0	-1	1	∞

cases as its maximum frequency can be improved by increasing the value of α. In Case 4, perfect position tracking is achieved at any frequencies and with any α.

D. Force Tracking Considering Actuator Saturation

To further investigate the effect of α on the shape of $1/f_{12}$ when r_m/r_s is very small and $\omega_m = \omega_s$, the magnitudes of $1/f_{12}$ for the four cases are plotted in Fig. 7 with $r_m = 0.01$, $R_s = 0.1$, $r_s = 10$, $\omega_m = \omega_s = \omega_0 = 100$ rad/s, $\alpha = 10, 50, 100, 500$.

When α is small (=10), the frequency ranges for ideal force tracking are limited for all cases, while when α is moderate or more (close to or greater than ω_m), these frequency ranges become wider and remain steady regardless of α. Moreover, in Case 1 and 2, force tracking is possible only at low frequencies (the frequency range of force tracking for Case 2 is a little wider than that for Case 1). In Case 3 (Fig. 7(c)), force tracking is satisfactory only at low frequencies, but the frequency range of $1/f_{12}$ can be improved by increasing α. In Case 4, good force tracking is achieved at any frequencies when α is not too small. Therefore, given very small r_m/r_s, perfect force tracking is possible without infinitely large α. Ideally, if $r_m = 0$ and $r_s = \infty$ are chosen, perfect free-motion transmitted impedance (h_{11}) can be attained for all cases, and perfect hard-contact transmitted impedance (z_{11}) can be achieved except for Case 1 (For Case 1, $z_{11} = k_{fs}$).

Based on the above analysis, it can be concluded that (a) for h_{11}, in all cases, the human operator will only feel the reference impedance model for the master robot (Z_m), which means decreasing m_m and ω_m in Z_m will lead to ideal free-motion transmitted impedance; (b) for h_{21}, the ideal position tracking for Case 4 can be attained at any frequencies regardless of α; for Case 3, the performance is better than those of Case 1 and 2 as the maximum frequency can be improved by increasing α. Also, regardless of α, the frequency range of position tracking for Case 2 is a bit wider than that for Case 1; (c) for $1/f_{12}$, to obtain a wider frequency range of force tracking, a moderate α (close to or greater than ω_m) is needed for all cases. Like h_{21}, the ideal force tracking is satisfactory for Case 4 at any frequencies and for the other cases at low frequencies. Moreover, the maximum frequency for Case 3 can be improved by increasing α; (d) for z_{11}, except Case 1, the human operator will only feel the impedance models for the master and slave robots. In Case 1, however, the slave flexibility will be transmitted to the human operator.

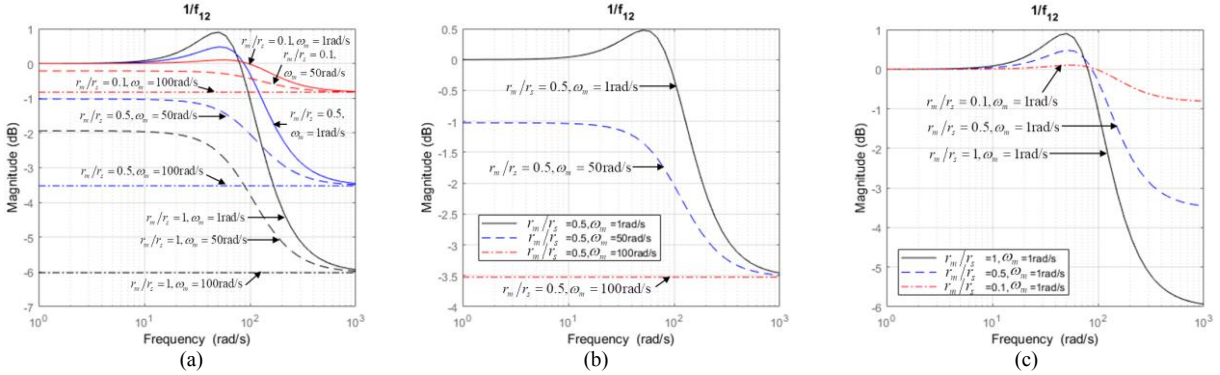

Figure 5. (a) Magnitudes of $1/f_{12}$ for case 3 (a) when r_m/r_s = 1, 0.5, 0.1, ω_s = 100 rad/s, ω_m = 1, 50, 100 rad/s. (b) When r_m/r_s is a constant (as an expample r_m/r_s= 0.5), the magnitude of $1/f_{12}$ with ω_m = 1, 50, 100 rad/s. (c) When ω_m is 1 rad/s, the magnitude of $1/f_{12}$ with r_m/r_s = 1, 0.5, 0.1.

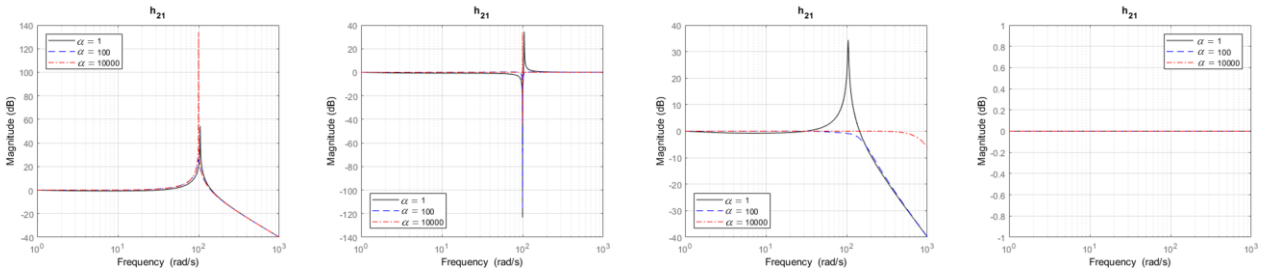

Figure 6. Magnitudes of h_{21} for (a) Case 1, (b) Case 2, (c) Case 3, and (d) Case 4 when ω_0 = 100 rad/s, R_s = 0.1, and α = 1, 100, 10000.

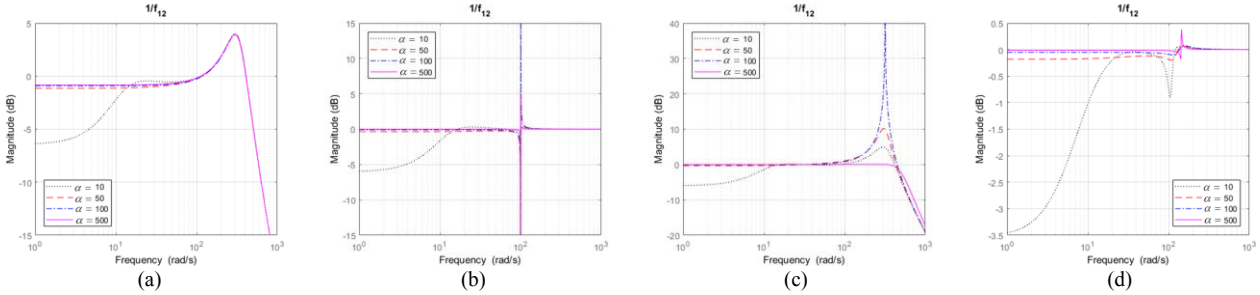

Figure 7. Magnitudes of $1/f_{12}$ for Case (a) 1, (b) 2, (c) 3, and (d) 4 when r_m = 0.01, R_s = 0.1, r_s = 10, $\omega_m = \omega_s = \omega_0$ =100 rad/s, α = 10, 50, 100, 500.

V. Simulation Study

The teleoperation system is simulated in MATLAB and Simulink. As an example, the results for Case 1 are presented in Fig. 8. Here, $M_m = M_{sm} = 1$ kg, $M_{se} = 0.1$ kg, $m_m = 0.01$ kg, $m_s = 10$ kg, $c_m = 2$ Ns/m, $c_s = 2 \times 10^3$Ns/m, $k_m = 100$ N/m, $k_s = 10^5$ N/m, $k_{fs} = 10^3$ N/m, and $\alpha = 100$ are chosen. Therefore, $R_s = 0.1$, $r_m = 0.01$, $r_s = 10$, $\zeta_m = \zeta_s = 1$, $\omega_m = \omega_{sm} = \omega_0 = 100$ rad/s. To achieve a rich and uniform spectrum over the frequency range of interest, the input f_h was designed to be the sum of several sinusoids evenly spaced in the frequency domain from 0 to 1000 rad/s. The simulations for free-motion and hard-contact were implemented when $k_e = 0$ N/m and $k_e = 10^6$ N/m, respectively. The recorded data from Simulink were applied spectral analysis to obtain the estimated magnitudes of the measures of transparency (Fig. 8). Without infinite α all the estimated lines (dotted) closely follow the idealized measures listed in the second row of Table II (solid).

VI. Conclusion

The control of a mechatronic-assisted system for surgeries with flexible tools and the effect of robot flexibility on the proposed bilateral impedance-controlled teleoperation system with different feedback and feedforward signals were studied. The parameter adjustment of the impedance models for the master and slave robots was analyzed and can be concluded that r_m/r_s should be very small if $\omega_m = \omega_s$ is desired. With the adjustment, it was shown that with the knowledge of the slave motor and tip positions (Case 4), perfect position and force tracking could be attained at any frequencies regardless of the control gain α (as long as α is not too small); otherwise, position and force tracking are possible only at low frequencies. Moreover, with the feedback of the slave tip position (Case 3), the frequency ranges of the measures can be improved by increasing the control gain. Also, regardless of the control gain, when the feedback position only involved the slave motor position, the case with accurate reference position for the slave motor (Case 2) has a bit wider frequency ranges of the measures than the other case (Case 1). By comparing the transparency measures of the proposed bilateral impedance-controlled teleoperation system with the measures of the conventional PEB and DFR teleoperation architectures presented in [13], the conclusion can be drawn that by using the adjusted parameters of the reference impedance models for the master and slave robots and considering actuator saturation, the proposed mechatronic-assisted teleoperation system can attain ideal transparency.

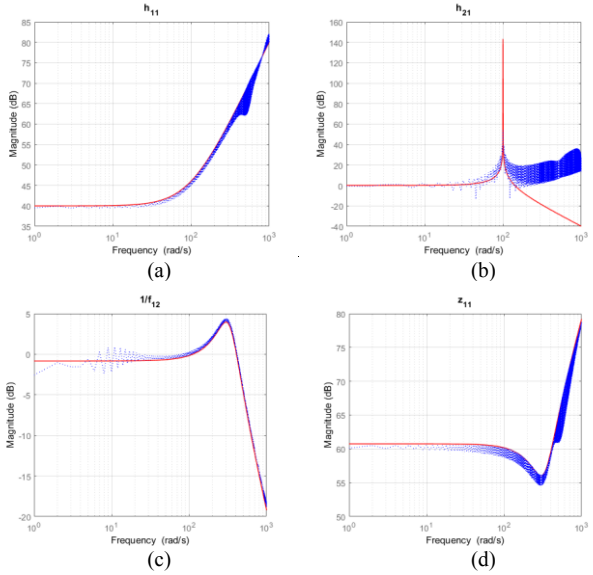

Figure 8. Magnitudes of (a) h_{11}, (b) h_{21}, (c) $1/f_{12}$, and (d) z_{11} for case 1.

Acknowledgements

Research supported by the Canada Foundation for Innovation (CFI) under grant LOF 28241 and JELF 35916, the Natural Sciences and Engineering Research Council (NSERC) of Canada under grant RGPIN 372042, and the China Scholarship Council (CSC) under grant [2015]08410152.

References

[1] S. A. Centenero and F. Hernández-alfaro, "3D planning in orthognathic surgery : CAD / CAM surgical splints and prediction of the soft and hard tissues results e Our experience in 16 cases," *J. Cranio-Maxillofacial Surg.*, vol. 40, no. 2, pp. 162–168, 2012.

[2] S. Gillen *et al.*, "Solo-surgical laparoscopic cholecystectomy with a joystick-guided camera device : a case – control study," *Surg. Endosc. Other Interv. Tech.*, vol. 28, pp. 164–170, 2014.

[3] J. Luo, C. Yang, and S. Dai, "Tremor attenuation for surgical robots using support vector machine with parameters optimization," *2018 Tenth Int. Conf. Adv. Comput. Intell.*, pp. 667–672, 2018.

[4] P. Kazanzides, Z. Chen, A. Deguet, G. S. Fischer, R. H. Taylor, and S. P. Dimaio, "An Open-Source Research Kit for the da Vinci Surgical System," *2014 IEEE Int. Conf. Robot. Autom.*, pp. 6434–6439, 2014.

[5] A. J. Hung, J. Chen, A. Shah, and I. S. Gill, "Review Article Telementoring and Telesurgery for Minimally Invasive Procedures," *J. Urol.*, vol. 199, no. 2, pp. 355–369, 2018.

[6] M. Tavakoli, A. Aziminejad, R. V. Patel, and M. Moallem, "High-fidelity bilateral teleoperation systems and the effect of multimodal haptics," *IEEE Trans. Syst. Man, Cybern. Part B Cybern.*, vol. 37, no. 6, pp. 1512–1528, 2007.

[7] L. Cheng, M. Sharifi, and M. Tavakoli, "Towards robot-assisted anchor deployment in beating-heart mitral valve surgery," *Int. J. Med. Robot. Comput. Assist. Surg.*, vol. 14, no. 3, pp. 1–10, 2018.

[8] L. Cheng and M. Tavakoli, "Switched-Impedance Control of Surgical Robots in Teleoperated Beating-Heart Surgery," *J. Med. Robot. Res.*, pp. 1841003, 2018.

[9] L. Cheng and M. Tavakoli, "Ultrasound image guidance and robot impedance control for beating-heart surgery," *Control Eng. Pract.*, vol. 81, pp. 9–17, 2018.

[10] S. K. Dwivedy and P. Eberhard, "Dynamic analysis of flexible manipulators, a literature review," *Mech. Mach. Theory*, vol. 41, no. 7, pp. 749–777, 2006.

[11] M. Mahvash and P. E. Dupont, "Bilateral Teleoperation of Flexible Surgical Robots," in *Proceedings of the New Vistas and Challenges in Telerobotics Workshop, IEEE 2008, International Conference on Robotics & Automation*, pp. 19–23, 2008.

[12] S. F. Atashzar, M. Shahbazi, H. A. Talebi, and R. V. Patel, "Control of time-delayed telerobotic systems with flexible-link slave manipulators," in *IEEE International Conference on Intelligent Robots and Systems*, vol. 1, no. 1, pp. 3035–3040, 2012.

[13] M. Tavakoli and R. D. Howe, "Haptic Effects of Surgical Teleoperator Flexibility," *Int. J. Rob. Res.*, vol. 28, no. 10, pp. 1289–1302, 2009.

[14] G. Zhu, S. S. Ge, and T. H. Lee, "Simulation studies of tip tracking control of a single-link flexible robot based on a lumped model," *Robotica*, vol. 17, no. 1, pp. 71–78, 1999.

[15] C. Pacchierotti, M. Abayazid, S. Misra, and D. Prattichizzo, "Teleoperation of steerable flexible needles by combining kinesthetic and vibratory feedback," *IEEE Trans. Haptics*, vol. 7, no. 4, pp. 551–556, 2014.

[16] S. E. Talole, J. P. Kolhe, and S. B. Phadke, "Extended-state-observer-based control of flexible-joint system with experimental validation," *IEEE Trans. Ind. Electron.*, vol. 57, no. 4, pp. 1411–1419, 2010.